Probing $\mu e\gamma\gamma$ contact interactions with $\mu \to e$ conversion

Sacha Davidson, Yoshitaka Kuno, Yuichi Uesaka, Masato Yamanaka

Probing $\mu e\gamma\gamma$ contact interactions with $\mu \to e$ conversion

S. Davidson,[1,*] Y. Kuno,[2,3,†] Y. Uesaka,[4,‡] and M. Yamanaka[5,6,§]

[1] *LUPM, CNRS, Université Montpellier, Place Eugene Bataillon, F-34095 Montpellier, Cedex 5, France*
[2] *Department for Physics, Osaka University, Osaka 560-0043, Japan*
[3] *Research Center of Nuclear Physics, Osaka University, Osaka 567-0047, Japan*
[4] *Faculty of Science and Engineering, Kyushu Sangyo University, 2-3-1 Matsukadai, Higashi-ku, Fukuoka 813-8503, Japan*
[5] *Department of Mathematics and Physics, Osaka City University, Osaka 558-8585, Japan*
[6] *Nambu Yoichiro Institute of Theoretical and Experimental Physics (NITEP), Osaka City University, Osaka 558-8585, Japan*

(Received 12 October 2020; accepted 7 December 2020; published 31 December 2020)

Contact interactions of a muon, an electron and two photons can contribute to the decay $\mu \to e\gamma\gamma$, but also to the conversion of a muon into an electron in the electric field of a nucleus. We calculate the $\mu \to e$ conversion rate, and show that for the coefficients of operators involving the combination $FF \propto |\vec{E}|^2$ (as opposed to $F\tilde{F} \propto \vec{E} \cdot \vec{B}$), the current bound on $\mu \to e$ conversion is more sensitive than the bound on $\mu \to e\gamma\gamma$.

DOI: 10.1103/PhysRevD.102.115043

I. INTRODUCTION

The observed neutrino masses imply the existence of contact interactions where charged leptons change flavor. This is referred to as (charged) lepton flavor violation (CLFV) and is reviewed for muon decays in, e.g., [1]. Current constraints on several $\mu \leftrightarrow e$ flavor changing processes are restrictive, and experiments under construction [2–4] aim to reach BR $\sim 10^{-16}$. Some bounds and future sensitivities are given in Table I.

If CLFV is discovered, experimental bounds on, or observations of, a multitude of independent processes would assist in discriminating among models. This motivates our interest in the less commonly considered contact interactions involving a muon, an electron and two photons. Such interactions could mediate various processes, such as $\mu \to e\gamma\gamma$ and $\mu \to e$ conversion in the electric field of a nucleus. The rate for $\mu \to e\gamma\gamma$ was calculated by Bowman, Cheng, Li and Matis (BCLM) [11], whose results are reviewed in Sec. II, and an experimental search with the Crystal Box detector obtained $\mathrm{BR}(\mu \to e\gamma\gamma) \leq 7.2 \times 10^{-11}$ [7]. Similar contact interactions, involving two photons but dark matter instead of leptons, have been studied in [12–15].

We will parametrize CLFV interactions via contact interactions involving Standard Model (SM) particles. This would be appropriate if the new particles involved in CLFV are heavy, but may not be generic for $\mu \to e\gamma\gamma$. This decay could be mediated by $\mu \to ea$ [16] followed by $a \to \gamma\gamma$, where a is a light (pseudo) scalar such as an axionlike particle [17]. Recently, the MEG experiment searched for collinear photons from this process [18]. They found that the branching ratio of $\mu^+ \to e^+ a, a \to \gamma\gamma$ is smaller than $\mathcal{O}(10^{-11})$ when the mediator a has a mass of 20–45 MeV and a lifetime below 40 ps.

In this manuscript, we calculate the $\mu \to e$ conversion rate induced by contact interactions of μ, e and two photons. Section II introduces the basis of operators (previously given by BCLM [11]), and gives their contribution to $\mu \to e\gamma\gamma$. The operators are of dimension seven and eight; we focus on the dimension seven operators, which can arise from loop corrections to dimension six scalar operators. Our calculation of $\mu \to e$ conversion mediated by the $\bar{e}\mu FF$ operator is presented in Secs. III and IV, where we first calculate the interaction of the leptons with the classical electromagnetic field, then in Sec. IV find a surprisingly large "short distance" loop interaction of two photons with individual protons. The final discussion section integrates our results in the usual expression for the spin independent branching ratio of $\mu \to e$ conversion, and discusses the current and future sensitivity to the $\bar{e}\mu FF$ operator coefficients at the experimental scale. Appendix A considers loop contributions to the $\bar{e}\mu FF$ operator and its relation to dimension six LFV

*s.davidson@lupm.in2p3.fr
†kuno@phys.sci.osaka-u.ac.jp
‡uesaka@ip.kyusan-u.ac.jp
§yamanaka@osaka-cu.ac.jp

TABLE I. Current bounds on the branching ratios for various CLFV processes, and the expected reach of upcoming experiments.

Process	Current sensitivity	Future
$\mu \to e\gamma$	$<4.2 \times 10^{-13}$ (MEG [5])	$\sim 10^{-14}$ (MEG II [6])
$\mu \to e\gamma\gamma$	$<7.2 \times 10^{-11}$ (Crystal Box [7])	$\sim 10^{-16}$ (Mu3e [4])
$\mu \to e\bar{e}e$	$<1.0 \times 10^{-12}$ (SINDRUM [8])	$\sim 10^{-16}$ (COMET [2], Mu2e [3])
$\mu A \to eA$	$<7 \times 10^{-13}$ (SINDRUM II [9])	$\sim 10^{-18}$ (PRISM/PRIME [10])

operators in models of heavy new physics (and in passing mentions an accidental cancellation in the contribution of the LFV Higgs coupling operator $\mathcal{O}_{EH}$ to $\mu \to e$ conversion). Appendix B shows the numerical values of the overlap integral which will be introduced in Sec. III.

II. NOTATION AND REVIEW

A set of QED-invariant operators that could mediate the decay $\mu \to e\gamma\gamma$ was given by Bowman, Cheng, Li and Matis (BCLM) [11]:

$$\begin{aligned}\delta\mathcal{L} = &\frac{1}{v^3}(C_{FF,L}\bar{e}P_L\mu F_{\alpha\beta}F^{\alpha\beta} + C_{FF,R}\bar{e}P_R\mu F_{\alpha\beta}F^{\alpha\beta} + C_{F\tilde{F},L}\bar{e}P_L\mu F_{\alpha\beta}\tilde{F}^{\alpha\beta} + C_{F\tilde{F},R}\bar{e}P_R\mu F_{\alpha\beta}\tilde{F}^{\alpha\beta})\\ &+\frac{1}{v^4}(C_{VFF,L}\bar{e}\gamma^\sigma P_L\mu F^{\alpha\beta}\partial_\beta F_{\alpha\sigma} + C_{VFF,R}\bar{e}\gamma^\sigma P_R\mu F^{\alpha\beta}\partial_\beta F_{\alpha\sigma}\\ &+ C_{VF\tilde{F},L}\bar{e}\gamma^\sigma P_L\mu F^{\alpha\beta}\partial_\beta\tilde{F}_{\alpha\sigma} + C_{VF\tilde{F},R}\bar{e}\gamma^\sigma P_R\mu F^{\alpha\beta}\partial_\beta\tilde{F}_{\alpha\sigma}) + [\mathrm{H.c.}], \end{aligned} \tag{1}$$

where two changes have been made to their notation: the new physics scale in the denominator is taken to be the Higgs vacuum expectation value $v \simeq m_t$, with $2\sqrt{2}G_F = 1/v^2$ (BCLM took m_μ), and we use chiral fermions, because this facilitates matching onto the full SM at the weak scale, and because the outgoing electrons are relativistic so $\approx$ chiral.

This basis of operators is constructed to include all possible Lorentz contractions that give the desired external particles (there is no tensor, because there is no two-index antisymmetric combination of FF or $F\tilde{F}$ to contract with $\bar{e}\sigma\mu$[1]), so corresponds to a general parametrization of the interaction at lowest order in a momentum expansion. The resulting operators are of dimension seven and eight.

Curiously, all the operators of Eq. (1) induce a matrix-element-squared for $\mu(P_\mu) \to e(p_e) + \gamma(k) + \gamma(q)$ that is proportional to [11]

$$|\mathcal{M}|^2 \propto P_\mu \cdot p_e (k \cdot q)^2,$$

giving a branching ratio

$$\mathrm{BR}(\mu \to e\gamma\gamma) = C^2 \frac{2m_\mu^2}{5v^2}, \tag{2}$$

where

$$\begin{aligned}C^2 = &\left|C_{FF,L} + i\frac{m_\mu C_{VFF,R}}{4v}\right|^2 + \left|C_{FF,R} + i\frac{m_\mu C_{VFF,L}}{4v}\right|^2\\ &+\left|C_{F\tilde{F},L} + i\frac{m_\mu C_{VF\tilde{F},R}}{2v}\right|^2\\ &+\left|C_{F\tilde{F},R} + i\frac{m_\mu C_{VF\tilde{F},L}}{2v}\right|^2 \end{aligned} \tag{3}$$

The experimental bound from Crystal Box [7] given in Table I therefore corresponds to

$$\frac{m_\mu}{v}|C| \lesssim 1.3 \times 10^{-5} \Rightarrow |C| \lesssim 2.2 \times 10^{-2}. \tag{4}$$

Notice that the BCLM study focuses on "short-distance" contributions to $\mu \to e\gamma\gamma$ mediated by LFV contact interactions. There could also be a "long-distance" contribution, induced by a LFV four-fermion operator that coupled $\bar{e}\mu$ to the neutral pion, which decays to $\gamma\gamma$. This process could have more interesting sensitivity to the relevant pseudo-scalar four-fermion operator that KTEV [19] (because the muon decays weakly, but the π_0 decays electromagnetically), but we do not consider it further here because we are interested in $\mu \to e$ conversion, and the π_0 couples to $\vec{E} \cdot \vec{B}$, which is negligibly small in the nucleus. Consequently, we disregard $\vec{E} \cdot \vec{B}$ contributions in the remainder of this paper.

In many heavy new physics models, LFV arises at dimension six. So for a sufficiently high new physics scale Λ_{NP}, it is reasonable to neglect the dimension ≥ 7 operators that could be generated at Λ_{NP}, because their contributions

[1]The tensor operator considered in [14] should vanish.

to observables will be suppressed by additional factors of $E_{\rm expt}/\Lambda_{\rm NP}$. However, some of the operators of Eq. (1) can arise at $\mathcal{O}(1/\Lambda_{\rm NP}^2)$ in a CLFV new physics model, with a SM mass scale providing the additional dimensions in the denominator. For example, if the scalar operators

$$\mathcal{O}^{\psi\psi}_{S,XX} \equiv (\bar{e}P_X\mu)(\bar{\psi}P_X\psi), \quad \mathcal{O}^{\psi\psi}_{S,XY} \equiv (\bar{e}P_X\mu)(\bar{\psi}P_Y\psi) \tag{5}$$

are present in the Lagrangian as $\delta\mathcal{L} = \frac{1}{\Lambda_{\rm NP}^2}(C^{\psi\psi}_{S,XX}\mathcal{O}^{\psi\psi}_{S,XX} + C^{\psi\psi}_{S,XY}\mathcal{O}^{\psi\psi}_{S,XY})$, then at a heavy fermion mass scale m_ψ, they match onto the two-photon operator $\mathcal{O}_{FF,X}$ via the diagram of Fig. 1, with coefficient

$$\frac{C_{FF,X}}{v^3} = -\sum_\psi (C^{\psi\psi}_{S,XX} + C^{\psi\psi}_{S,XY})\frac{Q_\psi^2 N_c \alpha_e}{12\pi m_\psi \Lambda_{\rm NP}^2} \tag{6}$$

where $N_c = 3$ for heavy quarks, and is one otherwise. This result is related to the conformal anomaly [20], and is the QED version of the matching of scalar heavy quark operators onto gluons, performed by Shifman, Vainshtein and Zakharov [21] (the $\bar{e}\mu GG$ operators were included in $\mu \to e$ conversion by [22]).

The dimension eight two-photon operators $\mathcal{O}_{VFF,X} = \bar{e}\gamma^\sigma P_X \mu F^{\alpha\beta}\partial_\beta \tilde{F}_{\alpha\sigma}$ appear more difficult to obtain at $\mathcal{O}(1/\Lambda_{\rm NP}^2)$. Furry's theorem says that dimension six vector operators, such as $(\bar{e}\gamma^\alpha P_X\mu)(\bar{\psi}\gamma_\alpha\psi)$, do not match onto $\mathcal{O}_{VFF,X}$ via the diagram of Fig. 1, because an odd number of vector current insertions appear on the fermion loop. Writing the loop of Fig. 1 with external legs amputated and an axial heavy fermion current $(\bar{e}\gamma^\alpha P_X\mu)(\bar{\psi}\gamma_\alpha\gamma_5\psi)$ in the grey blob, gives a vacuum matrix element that is even under charge conjugation, but odd under CP. Analogously to Furry's theorem, it should vanish in a CP invariant theory, so we do not calculate this diagram in the approximation of CP invariance.

In the next sections, we attempt to calculate the contribution of the scalar $\mathcal{O}_{FF,X}$ operators to coherent $\mu \to e$ conversion. The new physics scale is not required to be particularly high: Sec. III considers the "long-range" classical electromagnetic field of the nucleus, and should be valid for $\Lambda_{\rm NP}$ such that $\mathcal{O}_{FF,X}$ is a contact interaction at the muon mass scale. Section IV is a QED loop calculation

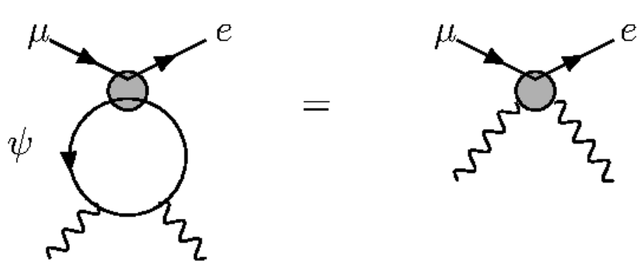

FIG. 1. Matching of scalar heavy fermion operators $\mathcal{O}^{\psi\psi}_{S,XY}$, $\mathcal{O}^{\psi\psi}_{S,XX}$ onto the two-photon operator $\mathcal{O}_{FF,X}$.

involving protons, which requires $\Lambda_{\rm NP} \gg m_p$. In Appendix A, we will reconsider the case of $\Lambda_{\rm NP} \gg m_W$. We do not consider the contribution of the dimension eight $\mathcal{O}_{VFF,X}$ operators; if new physics scale is high, their contribution to $\mu \to e$ conversion would be relatively suppressed by $\mathcal{O}(E_{\rm expt}^2/\Lambda_{\rm NP}^2)$ compared to that of dimension six LFV operators, and we are not aware of a motivated light new physics model that induces these operators.

III. THE $\mu \to e$ CONVERSION RATE IN THE CLASSICAL ELECTRIC FIELD

We consider the coherent $\mu \to e$ conversion described by the first two terms of Eq. (1). Assuming that the muon and the outgoing electron are independently described by their wave functions in a Coulomb potential, the transition matrix is

$$\mathcal{M} = \frac{1}{v^3}\int d^3r \bar{\psi}_e(\boldsymbol{r})(C_{FF,L}P_L + C_{FF,R}P_R) \times \psi_\mu^{1s}(\boldsymbol{r})\langle N|F_{\alpha\beta}F^{\alpha\beta}|N\rangle, \tag{7}$$

where ψ_μ^{1s} and ψ_e are respectively the wave functions of a $1s$ bound muon and the outgoing electron. Here, we omit spin indices for simplicity. $|N\rangle$ denotes the ground state of a nucleus. For an ordinary nucleus, we can safely assume that the electric field $\boldsymbol{E}(\boldsymbol{r})$ is spherically symmetric and the magnetic field is negligible.

We approximate the hadronic matrix element with a classical field strength as:

$$\langle N|F_{\alpha\beta}F^{\alpha\beta}|N\rangle = -2\{E(r)\}^2. \tag{8}$$

Diagrammatically, this corresponds to assuming that both exchanged photons carry three-momentum but no energy (giving a Coulomb potential), and neglects excited intermediate states for the nucleus. It can be compared to the approximation of Weiner and Yavin [13] for dark matter scattering on nuclei, where the nucleus is treated as a particle of charge Z in heavy quark effective theory, with a form factor to account for its finite size.[2]

With the amplitude $\mathcal{M}$, the conversion probability is given by

$$d\Gamma_{\rm conv} = \frac{d^3p_e}{(2\pi)^3 2E_e}(2\pi)\delta(E_e - E_e^{\rm conv})\overline{\sum_{\rm spins}}|\mathcal{M}|^2, \tag{9}$$

where the summation includes spin averaging of the initial state, and $E_e^{\rm conv}$ is the energy of the signal electron, given by $E_e^{\rm conv} = [(m_N + m_\mu - B_\mu)^2 - m_N^2 + m_e^2]/2(m_N + m_\mu - B_\mu)$. Here B_μ is the binding energy of initial muon in the muonic

[2]This approach is inconvenient in our case because the wave functions of the electrically charged muon and electron are easier to include in position space.

atom. The lepton wave functions ψ_ℓ ($\ell = e, \mu$) obey the Dirac equation in a nuclear Coulomb potential; our formulation below follows [23,24].

For a spherically symmetric potential, one can represent the wave function of the bound muon as

$$\psi_\mu^{1s}(\boldsymbol{r}) = \begin{pmatrix} G(r)\chi_{-1}^{s_\mu}(\hat{r}) \\ iF(r)\chi_{+1}^{s_\mu}(\hat{r}) \end{pmatrix}, \tag{10}$$

where χ is a two-component spherical spinor.[3] The differential equations for the radial wave functions $G(r)$ and $F(r)$ are obtained from the Dirac equation as follows,

$$\frac{dG(r)}{dr} - (E_\mu + m_\mu + eV_C(r))F(r) = 0, \tag{11}$$

$$\frac{dF(r)}{dr} + \frac{2}{r}F(r) + (E_\mu - m_\mu + eV_C(r))G(r) = 0. \tag{12}$$

The nuclear Coulomb potential V_C is calculated with a nuclear charge density $\rho(r)$ as,

$$V_C(r) = \int_0^\infty dr' r'^2 \rho(r') \left[\frac{\theta(r-r')}{r} + \frac{\theta(r'-r)}{r'}\right]. \tag{13}$$

For the nuclear density, we adopted two different models, the two-parameter-Fermi distribution (2pF) and three-parameter-Gaussian distribution (3pG), given by

$$\rho_{2\mathrm{pF}}(r) = \frac{\rho_0}{1+\exp\frac{r-c}{z}}, \quad \rho_{3\mathrm{pG}}(r) = \frac{\rho_0(1+\omega\frac{r^2}{c^2})}{1+\exp\frac{r^2-c^2}{z^2}}. \tag{14}$$

The normalization has been used such that $Ze = 4\pi\int_0^\infty \rho(r)r^2 dr$ with the normalization factors ρ_0 for each type of distribution. The parameters, ω, c and z, are listed in Refs. [25,26].

For simplicity of formulation, we express the wave function of the outgoing electron of momentum $\vec{p}_e$ using the partial wave expansion:

$$\psi_e(\boldsymbol{r}) = \sum_{\kappa,\nu,m} 4\pi i^{l_\kappa}(l_\kappa, m, 1/2, s_e|j_\kappa, \nu) Y_{l_\kappa}^{m*}(\hat{p}_e) \times e^{-i\delta_\kappa}\begin{pmatrix} g^\kappa(r)\chi_\kappa^\nu(\hat{r}) \\ if^\kappa(r)\chi_{-\kappa}^\nu(\hat{r}) \end{pmatrix}, \tag{15}$$

where j_κ and l_κ are the total and orbital angular momentum, respectively. We introduced an integer quantum number κ that runs from $-\infty \to \infty$ skipping 0, and determines j and l as $j_\kappa = |\kappa| - 1/2$ and $l_\kappa = j_\kappa + \kappa/2|\kappa|$. Due to angular momentum conservation, only the waves with $\kappa = \mp 1$ contributes to $\mu \to e$ conversion. δ_κ is a phase shift of the κ partial wave, and the incoming boundary condition is taken from [24]. $(l_\kappa, m, 1/2, s_e|j_\kappa, \nu)$ is the Clebsch-Gordan coefficient, and $Y_{l_\kappa}^m(\hat{p}_e)$ is a spherical harmonic. The radial Dirac equations for each partial wave are

$$\frac{dg^\kappa(r)}{dr} + \frac{1+\kappa}{r}g^\kappa(r) - (E_e + m_e + eV_C(r))f^\kappa(r) = 0, \tag{16}$$

$$\frac{df^\kappa(r)}{dr} + \frac{1-\kappa}{r}f^\kappa(r) + (E_e - m_e + eV_C(r))g^\kappa(r) = 0. \tag{17}$$

The normalization of the wave functions is the same as Ref. [23].

Then the conversion probability is

$$\Gamma_{\mathrm{conv}} = 16G_F^2 m_\mu^5 \left\{\left|\frac{m_\mu}{v}(C_{FF,L} + C_{FF,R})F_A^-\right|^2 + \left|\frac{m_\mu}{v}(C_{FF,L} - C_{FF,R})F_A^+\right|^2\right\} \tag{18}$$

where the overlap integrals F_A^- and F_A^+ for a target nucleus A are

$$F_A^- = \frac{1}{\sqrt{2m_\mu^7}}\int_0^\infty dr r^2\{E(r)\}^2\{g^{-1}(r)G(r) - f^{-1}(r)F(r)\}, \tag{19}$$

$$F_A^+ = \frac{1}{\sqrt{2m_\mu^7}}\int_0^\infty dr r^2\{E(r)\}^2\{f^{+1}(r)G(r) + g^{+1}(r)F(r)\}. \tag{20}$$

Neglecting the electron mass, we have $g^{+1} = -f^{-1}$ and $f^{+1} = g^{-1}$, so $F_A^+ = F_A^- \equiv F_A$. For instance, F_A for aluminum ($Z = 13$) and gold ($Z = 79$) are 3.8×10^{-4} and -6.1×10^{-3}, respectively. F_A for other targets are listed in Appendix B, and the absolute values are plotted in Fig. 2.

A few nuclei are modeled by both the 2pF and 3pG distributions, in which case we give the results with the latest distribution. Apart from the dip around $Z = 38$ (discussed below), different distribution models lead to the same results within $\mathcal{O}(1)\%$ accuracy. The magnitude of F_A continues to grow at large Z (unlike other overlap integrals [23]), because the squared electric field of heavy nuclei $E(r)^2 \propto Z^2$.

In Fig. 2, one sees a dip in the overlap integral in the range $30 \lesssim Z \lesssim 50$. In order to interpret this cancellation, the integrand of F_A is plotted as a function of radius in Fig. 3 for $Z = 13$, 38, and 79. The oscillations arise from the electron wave function g^{-1}, whose first node is at

[3]The subscript is the eigenvalue of $\kappa = -\sigma\cdot\vec{L} - 1 = \pm(j+1/2)$, which is $-l-1$ when κ is negative, l when κ is positive. Unlike the four-component spinor ψ, the two-component spinors are L^2 eigenstates, with different L^2 eigenvalues in the upper and lower components. See [24] for the construction of these states.

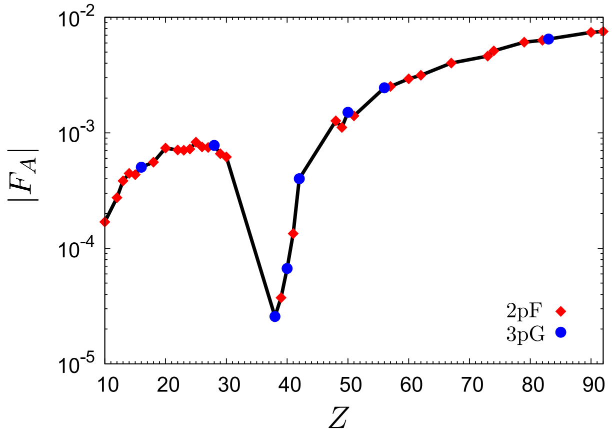

FIG. 2. $|F_A|$ as a function of atomic number (Z) for the target nucleus. Nuclear distributions are 3pG for $Z = 16$, 28, 38, 40, 42, 50, 56, and 83 (blue circle), and 2pF for other nuclei (red diamond).

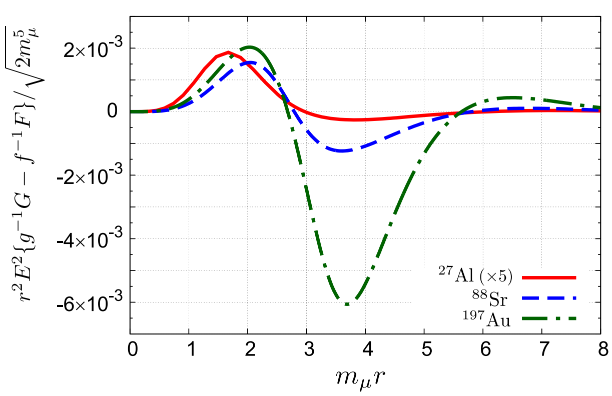

FIG. 3. Integrand of F_A for $Z = 13$, 38, and 79. The horizontal axis shows the dimensionless distance from a nuclear center. The amplitude for $Z = 13$ is multiplied by a factor 5.

$r \simeq \pi/m_\mu \simeq 5.8$ fm. Since the electric field is maximized around the nuclear surface, there is a significant cancellation between the interior and exterior contributions to the integral when the first node of g^{-1} is close to the nuclear radius. As a result, the overlap integral changes sign at $35 \lesssim Z \lesssim 40$, where the nuclear radius is about 5.5 fm.

However, the precise prediction of the dip is difficult, since the overlap integral at $30 \lesssim Z \lesssim 50$ is very sensitive to the nuclear model, and some parameters in the muonic atom (such as the muon binding energy at $\mathcal{O}(1)\%$ level). In order to reliably predict F_A for these targets, it would be necessary to model the nuclear distributions with considerable accuracy.

This interesting Z behavior could be a signature of the $\mathcal{O}_{FF,X}$ operators, if their contribution to the $\mu \to e$ conversion rate is dominant. For this reason we exhibit it. However, as discussed in the next section, there is a comparable loop contribution, which arises provided that the $\mu e\gamma\gamma$ interaction remains a contact interaction up to scales of a few GeV.

IV. TWO-PHOTON EXCHANGE WITH A PROTON

The nuclear matrix element of the FF operator involves the expectation value of two nucleon currents, which can be challenging to calculate. If the nucleus is represented as a nonrelativistic bound state of protons (and neutrons), then Wick contractions give two diagrams for the interaction of the $\mathcal{O}_{FF,X}$ operator with the nucleus, which are illustrated in Fig. 4. The sum of both diagrams was calculated in the previous Sec. III, in the approximation that the protons remain in their energy levels of an external nuclear potential. This implies that the photons only carry three-momentum, so correspond to the Coulomb potential (which can be checked in the bound state formalism of Appendix B of [27]). This neglects excited intermediate states of the nucleus, which are possible although the final state nucleus should be in the ground state, in order to contribute to coherent $\mu \to e$ conversion. (We also neglect correlations between the two protons, which were considered in [15].) In this section, we focus on the left diagram, where both photons interact with the same proton, and estimate the contribution of off-shell photons via the renormalization group equations (RGEs) of QED below the proton mass scale. At first sight, this diagram appears negligible, because it is loop-suppressed ($\propto 1/(16\pi^2)$), and benefits from only one factor Z enhancement, as opposed to Z^2 for the tree diagram on the right.

In the RGEs of QED, the FF operator can mix to scalar operators $m_\psi \mathcal{O}^{\psi\psi}_{S,XX}$, $m_\psi \mathcal{O}^{\psi\psi}_{S,XY}$ [defined in Eq. (5)], for ψ a charged point particle. This corresponds to the log-enhanced part of the loop where both photons interact with the same proton, can be reliably computed in EFT, and was considered in [14] for ψ a heavy quark. In an EFT of leptons and hadrons below 2 GeV, we apply this result for ψ a proton, for scales between 2 GeV and $m_\mu \simeq$ the momentum exchange of $\mu \to e$ conversion, which gives

$$\Delta C^{pp}_{S,X}(m_\mu) = -\frac{6\alpha_{em} m_p}{\pi v} \ln\frac{2\ \mathrm{GeV}}{m_\mu} C_{FF,X}$$
$$\simeq -2.26 \times 10^{-4} C_{FF,X} \qquad (21)$$

where $C^{pp}_{S,X} = \frac{1}{2}(C^{pp}_{S,XL} + C^{pp}_{S,XR})$, and $C_{FF,X}$ is evaluated at 2 GeV. This mixing, with ψ a proton, is discussed in [15] but was not included in [14]. It can only be a rough approximation to this loop, because the not-log-enhanced contributions are unknown and difficult to estimate.

We can now calculate the contribution of $C_{FF,X}$ to $\mu \to e$ conversion. The branching ratio is

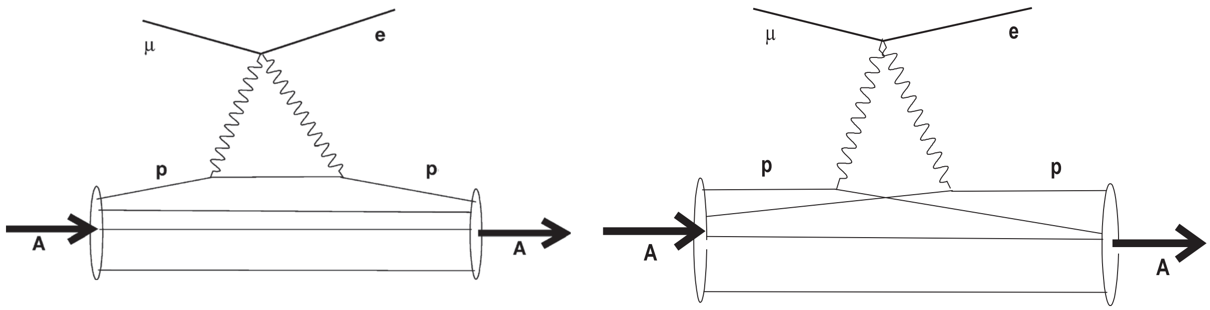

FIG. 4. Diagrams for two photons from the FF operator interacting with the nucleus A.

$$\mathrm{BR}(\mu A\to eA)=\frac{32G_F^2m_\mu^5}{\Gamma_{\mathrm{cap}}}\left[\left|\ldots+C_{S,L}^{pp}S_A^{(p)}+C_{S,L}^{nn}S_A^{(n)}+C_{D,L}\frac{D_A}{4}-\frac{m_\mu}{v}C_{FF,L}F_A\right|^2+\{L\leftrightarrow R\}\right] \tag{22}$$

where Γ_{cap} is the muon capture rate in a muonic atom [28], $S_A^{(N)}$ and D_A are respectively the overlap integrals in nucleus A of the $\bar{N}N$ nucleon current and the dipole operator [23], F_A is the overlap integral for the FF operator from Sec. III, and "…" represents the vector coefficients that we do not discuss. If the principle source of $\mu\to e$ flavor change at a scale of 2 GeV is $\mathcal{O}_{FF,X}$, then on aluminum and gold, we have

$$\frac{\mathrm{BR}(\mu A\to eA)}{|C_{FF,L}|^2+|C_{FF,R}|^2}=\begin{cases}6.6\times10^{-9}|1+15|^2 & \text{for }^{27}\mathrm{Al}\\ 9.1\times10^{-8}|-1+3.8|^2 & \text{for }^{197}\mathrm{Au}\end{cases}. \tag{23}$$

where between the absolute values is first the tree contribution, then the loop. Unexpectedly, the loop contribution could be larger than the tree for light and heavy nuclei.

Let us briefly discuss how this can occur. Naively, the loop amplitude should be suppressed relative to the tree contribution by $1/(16\pi^2Z)$. However:

(i) the numerical factor from the loop is large: Eq. (21) is $\sim 2\alpha\log$, rather than being $\sim\frac{\alpha}{4\pi}\log$.

(ii) the classical amplitude is suppressed by $1/(4\pi)$, because the electric field of a point charge Z is $|\vec{E}(r)|=Ze/(4\pi r^2)$, so a factor 4π remains in the denominator when E^2 is integrated over the volume of the nucleus. Combined with the first effect, this compensates the $1/16\pi^2$ suppression.

(iii) the FF operator is of dimension seven, so the amplitude is proportional to an energy scale. For the loop, this is the proton mass, whereas for the classical process, it is a combination of the momentum transfer (m_μ) and the inverse nuclear radius, which turns out to be $\sim m_\mu/\pi^2$. So this ratio of energy scales (over)compensates the Z suppression of the loop.

Alternatively, the second point (and part of the third), can be seen by noticing that the overlap integral $S_A^{(p)}$ is large compared to F_A. For simplicity, we assume a uniform proton distribution $\rho\propto Z(\frac{4\pi}{3}R^3)^{-1}$ for a nuclear radius $R\sim 1.1A^{1/3}$ fm. Since the nuclear electric field is maximized around the nuclear surface, we approximate the electric field as one at the surface, $|\vec{E}(r)|\simeq Ze/(4\pi R^2)$. Hence, the ratio of the overlap integrals is $|F_A/S_A^{(p)}|\simeq 2m_\mu^{-1}[\frac{Ze}{4\pi R^2}]^2/[Z(\frac{4\pi}{3}R^3)^{-1}]=2Z\alpha/(3m_\mu R)\sim 0.02$ for ^{27}Al (0.06 for ^{197}Au), where the overall factor $2m_\mu^{-1}$ covers the typical scale of $\mu\to e$ conversion and the difference of normalization for overlap integrals between F_A and $S_A^{(p)}$ [23]. That is naive understanding that the overlap F_A is small compared to $S_A^{(p)}$. The numerical calculation tells us that the ratio is 0.02 for ^{27}Al (0.1 for ^{197}Au).

Figure 5 shows the branching ratios for targets of atomic number Z normalized by that for aluminium. The branching ratio via the scalar CLFV operator, $\mathcal{O}_{S,X}^{pp}=\bar{e}P_X\mu(\bar{p}p)$, is also shown to highlight the difference of Z dependence. Two features of the overlap integral F_A can be seen: first, it has an additional factor of Z, due to the extra $F^{\mu\nu}$, and second, it becomes negative at large Z. The first point is illustrated by the dashed line, showing the branching ratio induced only by the tree contribution of the $\bar{e}\mu FF$ operator, which continues to increase at large Z. This differs from the high-Z falloff of the branching ratios due to the familiar dipole, scalar or vector operators [23]. The solid line includes the tree and loop contributions of the $\bar{e}\mu FF$ operator, which interfere destructively at large Z, where F_A is negative but the scalar overlap integral is positive. This sign difference, combined with the increasing magnitude of F_A at large Z, causes the branching ratio to decrease for increasing $Z\gtrsim 50$. The shape and magnitude of this feature differ from the high-Z decrease of dipole, scalar or vector operators [23]. We stress that this feature could be

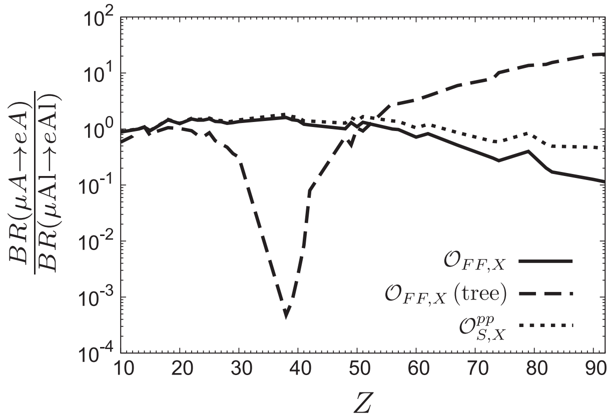

FIG. 5. Branching ratios for $\mu \to e$ conversion normalized to that for aluminum. The solid line shows the result for $\mathcal{O}_{FF,X} = \bar{e}P_X\mu F^{\alpha\beta}F_{\alpha\beta}$, where we consider two contributions: one is the interaction with the classical electric field of the nucleus, and the other is the effect of loop mixing of $\mathcal{O}_{FF,X}$ into $\mathcal{O}_{S,X} = (\bar{e}P_X\mu)(\bar{p}p)$ due to two-photon exchange. If neglecting the loop contribution, we obtain the dashed line. For comparison, the dotted line gives the normalized branching ratio for only the scalar operator $\mathcal{O}_{S,X}$.

used to discriminate the $\bar{e}\mu FF$ operator from other CLFV operators.

V. SUMMARY

In this manuscript, we calculated the contribution of low-energy $\bar{e}\mu\gamma\gamma$ contact interactions to $\mu \to e$ conversion on nuclei. We considered the first two operators of Eq. (1), which are CP-even, of dimension seven, and involve $F_{\mu\nu}F^{\mu\nu} \supset |\vec{E}|^2$. Other possibilities are discussed in Sec. II.

If the $\mu e\gamma\gamma$ interaction is a contact interaction at momentum transfers $\sim m_\mu$, then there is a contribution to $\mu \to e$ conversion from the leptons interacting with the electromagnetic field of the nucleus. The calculation is outlined in Sec. III. It relies on the overlap integrals in the nucleus, of the electron and muon wave functions with the electric-field-squared, which are given in Eqs. (19) and (20). This contribution has an interesting and rare feature: it changes sign at intermediate Z (=the electric charge of the target nucleus).

If the $\mu e\gamma\gamma$ interaction remains a contact interaction at larger momentum transfers $\gtrsim m_p$, then the dominant contribution of $\mathcal{O}_{FF,X}$ to $\mu \to e$ conversion arises from loop mixing into the scalar proton operator $\mathcal{O}_{S,X} = (\bar{e}P_X\mu)(\bar{p}p)$, as discussed in Sec. IV. Naively, the loop amplitude is suppressed by $1/(16\pi^2 Z)$, but overlap integrals, energy ratios, and numerical factors more than compensate, as discussed at the end of the section. The combined tree and loop contributions exhibit a unique Z-dependence that could be used to distinguish the $\bar{e}P_X\mu FF$ operator from other operators. The branching ratio for $\mu \to e$ conversion induced by $\mathcal{O}_{FF,X}$ is given in Eq. (22), and plotted in Fig. 5.

If the branching ratio for spin independent $\mu \to e$ conversion [23] is expressed as a function of operator coefficients at a scale of 2 GeV, our results for $\mathcal{O}_{FF,X}$ can be included as

$$\begin{aligned}\mathrm{BR}(\mu A \to eA) = \frac{32G_F^2 m_\mu^5}{\Gamma_{\mathrm{cap}}} \sum_{X\in\{L,R\}} \Bigg| & C_{D,X}\frac{D_A}{4} + (9.0C^{uu}_{S,X} + 8.2C^{dd}_{S,X} + 0.42C^{ss}_{S,X})S_A^{(p)} \\ & + (8.1C^{uu}_{S,X} + 9.0C^{dd}_{S,X} + 0.42C^{ss}_{S,X})S_A^{(n)} + \cdots \\ & - C_{GG,X}\frac{8\pi m_N}{9\alpha_s(2m_N)v}(0.90S_A^{(p)} + 0.89S_A^{(n)}) - C_{FF,X}\left(\frac{m_\mu}{v}F_A + \frac{18\alpha m_p}{\pi v}S_A^{(p)}\right)\Bigg|^2 \end{aligned} \tag{24}$$

where D_A and $S_A^{(N)}$ are the overlap integrals inside the nucleus A, with respectively the electric field or the appropriate nucleon ($N \in \{n,p\}$) distribution, which can be found in [23]. Γ_{cap} is the muon capture rate on nucleus A [28], $C_{D,X}$ is the dipole coefficient, $\{C^{qq}_{S,X}\}$ are the coefficients of $2\sqrt{2}G_F(\bar{e}P_X\mu)(\bar{q}q)$, and the "+…" represents the contributions of vector operators involving a light quark bilinear. This expression uses the quark densities in the nucleon of Refs.[4] [30–33], the gluon density [21,22]

$$\langle N|GG(x)|N\rangle \simeq \frac{8\pi m_N}{9\alpha_s(2\ \mathrm{GeV})}\langle N|\bar{N}N(x)|N\rangle, \tag{25}$$

and the last term gives the contribution of the operators $\mathcal{O}_{FF,X}$, at tree level via the overlap integral F_A tabulated in Appendix B, and via one loop mixing to the scalar proton density ($\ln(2\ \mathrm{GeV}/m_\mu) \simeq 3$ is used in the last term).

The SINDRUM II experiment searched for $\mu \to e$ conversion on gold, and obtained the upper bound $\mathrm{BR}(\mu\mathrm{Au} \to e\mathrm{Au}) \le 7\times 10^{-13}$ [9]. If we assume that only the "gauge boson operator" coefficients are nonzero (at a scale of 2 GeV), this corresponds to the bound:

$$4.9\times 10^{-8} \gtrsim |0.222C_{D,X} - 0.038C_{GG,X} - 4.8\times 10^{-5}C_{FF,X}|, \tag{26}$$

which gives, in the absence of $C_{D,X}$ and $C_{GG,X}$,

[4] These are the "EFT" determinations, which are ~50% larger than the lattice results [29].

TABLE II. $\mu\bar{e}\gamma\gamma$ operator coefficients bounded by $\mu \to e\gamma\gamma$ [7], and the sensitivity of μAu $\to e$Au [9] obtained in this manuscript. The operators are given in Eq. (1), $\{X, Y\} \in \{L, R\}$ with $X \neq Y$ and $v = 174$ GeV.

Coefficient	Constraint	Process
$\lvert C_{FF,X} + im_\mu C_{VFF,Y}/(4v)\rvert$	$<2.2 \times 10^{-2}$	$\mathrm{BR}(\mu \to e\gamma\gamma) < 7.2 \times 10^{-11}$
$\lvert C_{F\tilde{F},X} + im_\mu C_{VF\tilde{F},Y}/(4v)\rvert$	$<2.2 \times 10^{-2}$	$\mathrm{BR}(\mu \to e\gamma\gamma) < 7.2 \times 10^{-11}$
$\lvert \ldots + C_{FF,X}\rvert$	$<1.0 \times 10^{-3}$	$\mathrm{BR}(\mu\mathrm{Au} \to e\mathrm{Au}) < 7 \times 10^{-13}$

$$|C_{FF,X}| \leq 1.0 \times 10^{-3}. \tag{27}$$

This is a better sensitivity than that given in Eq. (4) from the Crystal Box search for $\mu \to e\gamma\gamma$. Searching for $\mu \to e\gamma\gamma$ nonetheless remains an interesting and complementary channel, because it probes all the operators of Eq. (1). Experimental constraints on $\mu\bar{e}\gamma\gamma$ coefficients are summarized in Table II.

The upcoming COMET and Mu2e experiments plan to start with an Aluminium target. Combining Eq. (24) and $F_{\mathrm{Al}} = 3.8 \times 10^{-4}$, we obtain a future sensitivity of

$$|C_{FF,X}| \leq 7.6 \times 10^{-6} \left(\frac{\mathrm{BR}(\mu\mathrm{Al} \to e\mathrm{Al})}{10^{-16}}\right)^{1/2}. \tag{28}$$

The sensitivity to $C_{FF,X}$ would be improved by two orders of magnitude with an expected branching ratio of $\sim 10^{-16}$ on the light target Aluminium.

Finally, we comment on the interest of the $(\bar{e}P_{L,R}\mu)FF$ operators in identifying heavy new physics in the lepton sector. These operators are of dimension seven in the QED $\times$ QCD-invariant EFT below m_W, and dimension eight above. However, they can be mediated by not-so-heavy, feebly coupled pseudoscalars of mass $m \gg m_\mu, m_p$, and in the case of new physics at scales $\gg m_W$, they can be induced in matching out heavy fermion scalar operators of dimension six, as illustrated in Fig. 1, and given in Eq. (5). However, the dominant contribution of such scalar operators to $\mu \to e$ conversion arises via the dipole or $(\bar{e}P_{L,R}\mu)GG$ operators. In Appendix A, we estimate the sensitivities of $\mu \to e\gamma$ and $\mu \to e$ conversion to scalar operators.

ACKNOWLEDGMENTS

We thank Jure Zupan and Lorenzo Calibbi for relevant comments on a first version of this manuscript. S. D. is happy to thank Vincenzo Cirigliano, Martin Gorbahn, Martin Hoferichter, Marc Knecht and Aneesh Manohar for useful conversations. We thank the IN2P3 and KEK for funding FJPPL-TYL-HEP-06, which made this manuscript possible. This work was supported by JSPS KAKENHI Grants No. JP18H05231 (Y. K.), No. JP18H01210 (Y. U.), and No. 20H05852 (M. Y.). This work was partly supported by MEXT Joint Usage/Research Center on Mathematics and Theoretical Physics JPMXP0619217849.

APPENDIX A: $\bar{e}\mu FF$ IN THE RGES

In this Appendix, we briefly consider how a heavy new physics model could induce the dimension seven FF operators. Parenthetically, we notice a partial cancellation in the contribution of LFV Higgs interactions to $\mu \to e$ conversion.

1. Obtaining $\bar{e}\mu FF$ at $\mathcal{O}(1/\Lambda_{\mathrm{NP}}^2)$

We assume that new physics generates dimension six CLFV operators at some scale $\Lambda_{\mathrm{NP}} > m_W$, which is high enough that dimension ≥ 7 operators can be neglected. Then $\mathcal{O}_{FF,X}$ can be generated in matching out dimension six operators, such as a Higgs with flavor-changing couplings, or a flavor-changing scalar operator involving heavy fermions.

We first consider the QED $\times$ QCD invariant EFT below m_W, in the notation of [34], where operators are added to the Lagrangian as $\mathcal{L}_{\mathrm{SM}} \to \mathcal{L}_{\mathrm{SM}} + 2\sqrt{2}G_F \Sigma C^\zeta_{Lor}\mathcal{O}^\zeta_{\mathrm{Lor}}$, with ζ being flavor indices, and the subscript giving the Lorentz structure. As illustrated in Fig. 1, the scalar operators $\mathcal{O}^{\psi\psi}_{S,XX}, \mathcal{O}^{\psi\psi}_{S,XY}$ [see Eq. (5)], match at m_ψ onto $\mathcal{O}_{FF,X}$ and $\mathcal{O}_{GG,X}$:

$$\frac{C_{FF,X}}{v} = -\frac{\alpha Q_\psi^2 N_{c,\psi}}{12\pi m_\psi(m_\psi)}(C^{\psi\psi}_{S,XX} + C^{\psi\psi}_{S,XY}) \tag{A1}$$

$$\frac{C_{GG,X}}{v} = -\frac{\alpha_s(m_Q)}{24\pi m_Q(m_Q)}(C^{QQ}_{S,XX} + C^{QQ}_{S,XY}) \tag{A2}$$

where $Q \in \{c, b, t\}$. We focus on $\psi \in \{\tau, c, b, t\}$ a heavy fermion, because the operators with $\psi \in \{e, u, d, s\}$ contribute at tree level to $\mu \to e$ conversion or $\mu \to e\bar{e}e$, and for $\psi = \mu$, the operator contributes at one loop to $\mu \to e\gamma$. It is interesting to pursue the loop effects of these heavy-fermion scalars, because the two heavy fermions make the operators difficult to probe directly in experiment.

The $\mathcal{O}^{\psi\psi}_{S,XX}$ scalar operators (with the same chiral projector in both bilinears) contribute to the dipole operator via "Barr-Zee" diagrams. The log^2-enhanced part is given by the one-loop RGEs of QED [35,36] as

$$\Delta C_{D,X} \approx 8\frac{\alpha_e^2}{e(4\pi)^2}\left(C^{\tau\tau}_{S,XX}\frac{m_\tau}{m_\mu}\ln^2\frac{m_W}{m_\tau} + \frac{4m_c}{3m_\mu}C^{cc}_{S,XX}\ln^2\frac{m_W}{m_c} + \frac{m_b}{3m_\mu}C^{bb}_{S,XX}\ln^2\frac{m_W}{m_b}\right) \tag{A3}$$

where $C_{D,X}$ is the dipole coefficient at the experimental scale, and the coefficients on the right are evaluated at m_W. Numerically, this is

$$\Delta C_{D,X} \approx 9\times 10^{-6}(245C^{\tau\tau}_{S,XX}+277C^{cc}_{S,XX}+117C^{bb}_{S,XX})$$

where the current MEG bound $\mathrm{BR}(\mu\to e\gamma)\leq 4.2\times 10^{-13}$ gives $C_{D,X}\lesssim 10^{-8}$. Comparing to Eqs. (A2) and (26), one sees that the scalar quark coefficients $C^{QQ}_{S,XX}$ give contributions to $\mu\to e$ conversion via the dipole and GG operators that are of the same order of magnitude and sign. So the SINDRUMII $\mu\to e$ conversion bound has better sensitivity to these operators [34] than the current MEG bound. On the other hand, $C^{\tau\tau}_{S,XX}$ contributes principally to $\mu\to e$ conversion via the dipole, rather than the FF operators, so high precision would be required to see the FF contribution, and MEG has better sensitivity.

The $\mathcal{O}^{\psi\psi}_{S,XY}$ operators can be Fierz-transformed to vector operators $-\frac{1}{2}(\bar{e}\gamma^\alpha\psi)(\bar{\psi}\gamma_\alpha\mu)$, which contribute to $\mu\to e\gamma$ at two-loop in EFT [36,37], that is $\mathcal{O}(\alpha_e^2\ln)$:

$$\begin{aligned}\Delta C_{D,X}\approx\frac{\alpha_e^2}{e(4\pi)^2}\Bigg[&\frac{58}{9}C^{\tau\tau}_{V,YY}+\frac{116}{9}\sum_{l=e,\mu}C^{ll}_{V,YY}\\&+\frac{64}{9}(C^{uu}_{V,YY}+C^{cc}_{V,YY})+\frac{22}{9}\sum_{q=d,s,b}C^{qq}_{V,YY}\\&-\frac{80}{9}(C^{uu}_{V,YX}+C^{cc}_{V,YX})-\frac{14}{9}\sum_{q=d,s,b}C^{qq}_{V,YX}\\&-\frac{50}{9}\sum_{l=e,\mu,\tau}C^{ll}_{V,YX}+4\sum_{f=b,c,s,\tau}C^{ff}_{S,YX}\frac{Q_f^2N_fm_f}{m_\mu}\Bigg]\ln\frac{m_W}{m_?}\end{aligned}\tag{A4}$$

where the logarithm should be inside the bracket, with a lower cutoff $\sim m_b\to m_\mu$ which depends on the operator. For the heavy quark coefficients $C^{QQ}_{S,XY}$, the contribution to $\mu\to e$ conversion via the $\mathcal{O}_{GG,X}$ operator is clearly larger than via the dipole or $\mathcal{O}_{FF,X}$ [see Eqs, (A2), (26)], giving the SINDRUMII search the best sensitivity.

For the tau scalar coefficient, Eq. (A4) corresponds to $\Delta C_{D,X}\simeq 2.9\times 10^{-4}C^{\tau\tau}_{S,YX}$ which gives $\mu\to e\gamma$ the current best sensitivity to this coefficient [34]. For $\mu\to e$ conversion, this contribution to the dipole can be compared with $\Delta C_{FF,X}\simeq 0.019C^{\tau\tau}_{S,YX}$ from Eq. (A2). Equation (26) then implies that the contribution of $C^{\tau\tau}_{S,YX}$ to $(\mu\mathrm{Au}\to e\mathrm{Au})$ via the dipole is an order of magnitude larger than via the FF operator, and a similar dominance of the dipole contribution arises in Aluminium. This can be understood diagrammatically, where both the contributions of $\mathcal{O}^{\tau\tau}_{S,YX}$ to the dipole, and to the scalar proton current, arise at 2-loop with a single log enhancement. However, the contributions to the dipole benefit from a m_τ/m_μ enhancement.

2. Of the sensitivity of $\mu\to e$ conversion to flavor-changing Higgs interactions

The discussion so far has been in the context of QED $\times$ QCD invariant operators below the weak scale. However, since we assume $\Lambda_{\rm NP}$ is large, it is relevant to translate to the SMEFT, where SU(2) invariance restricts the operator basis to three scalar four-fermion operators at dimension six: the XX scalar for u-type quarks, and the XY scalars for d-type quarks and charged leptons. There is also a flavor-changing Higgs coupling, which matches onto $\mathcal{O}_{FF,X}$ and $\mathcal{O}_{GG,X}$ at the weak scale. Including also the dipoles, these operators appear in the SMEFT Lagrangian as

$$\begin{aligned}\delta\mathcal{L}_{\rm SMEFT}=\frac{1}{v^2}(&C^{\mu e}_{\rm EH}H^\dagger H\bar{\ell}_\mu He+C^{e\mu}_{\rm EW}y_\beta(\bar{\ell}_e\tau^a H\sigma^{\mu\nu}e_\mu)W^a_{\mu\nu}\\&+C^{e\mu}_{\rm EB}y_\beta(\bar{\ell}_eH\sigma^{\mu\nu}e_\mu)B_{\mu\nu}+C^{e\tau\tau\mu}_{\rm LE}(\bar{\ell}_e\gamma^\mu\ell_\tau)(\bar{e}_\tau\gamma_\mu e_\mu)\\&+C^{\tau\mu e\tau}_{\rm LE}(\bar{\ell}_\tau\gamma^\mu\ell_\mu)(\bar{e}_e\gamma_\mu e_\tau)\\&+C^{e\mu nn}_{\rm LEQU}(\bar{\ell}^A_ee_\mu)\varepsilon_{AB}(\bar{q}^B_nu_n)\\&+C^{e\mu nn}_{\rm LEDQ}(\bar{\ell}_ee_\mu)(\bar{d}_nq_n))+\mathrm{H.c.},\end{aligned}\tag{A5}$$

where the capitalized SU(2) indices are explicit when not contracted in the parentheses, ℓ and q are doublets, u, d, e are singlets, flavor indices are superscripts, $n\in\{c,t,b\}$, and the operator labels are according to [38]. The $\mathcal{O}^{e\mu}_{\rm EW}$ and $\mathcal{O}^{e\mu}_{\rm EB}$ will combine to the dipole, the $\mathcal{O}_{\rm LE}$ operators Fiertz to XY scalar operators with a τ bilinear, and in the quark sector, $\mathcal{O}_{\rm LEQU}$ is a YY-scalar operator (same chiral projector twice), whereas $\mathcal{O}_{\rm LEDQ}$ is XY.

Loop effects between $\Lambda_{\rm NP}$ and the weak scale can be partially included via the RGEs of the SMEFT. Gauge boson loops can renormalize the coefficients, and mix the $C^{e\mu nn}_{\rm LEQU}$ coefficients into the u—type tensor operator, and then to the dipole (as occurs below m_W for YY scalars). Higgs exchange can mix these scalars into vector four-fermion operators (to which there could be better experimental sensitivity), but for $\mathcal{O}_{\rm LEDQ}$ and $\mathcal{O}_{\rm LE}$, this is negligible because suppressed by $\sim y_\mu y_\psi/(16\pi^2)$ ($\psi\in\{\tau,b\}$). We therefore suppose that the coefficients in Eq. (A5) are given at the weak scale m_W, since the one-loop RGEs above m_W do not appear to significantly mix the XY-scalars into more experimentally accessible operators.

The coefficients from Eq. (A5) can be matched at m_W onto those of QED $\times$ QCD-invariant scalar four-fermion operators, relevant at low energy. All the scalar operators below m_W are generated at tree level, just that some arise due to Higgs exchange with a flavor-changing coupling from the $\mathcal{O}_{\rm HE}$ operator, leading to correlations in the coefficients. One obtains [35]

$$C_{D,R}(m_W) = c_W C^{e\mu}_{\rm EB}(m_W) - s_W C^{e\mu}_{\rm EW}(m_W) + C^{e\mu}_{\rm EH}(m_W)\left[\frac{e\alpha y_t^2}{8\pi^3 y_\mu}\right] \tag{A6}$$

$$C^{\tau\tau}_{S,RR} = -\frac{m_\tau C^{e\mu}_{\rm EH} v}{m_h^2} \tag{A7}$$

$$C^{\tau\tau}_{S,LR} = -2C^{\tau\mu e\tau}_{\rm LE} - \frac{m_\tau C^{\mu e*}_{\rm EH} v}{m_h^2} \tag{A8}$$

$$C^{\tau\tau}_{S,RL} = -2C^{e\tau\tau\mu}_{\rm LE} - \frac{m_\tau C^{e\mu}_{\rm EH} v}{m_h^2} \tag{A9}$$

$$C^{\tau\tau}_{S,LL} = -\frac{m_\tau C^{\mu e*}_{\rm EH} v}{m_h^2} \tag{A10}$$

$$C^{cc}_{S,LL} = C^{*\mu ecc}_{\rm LEQU} - \frac{m_c v}{m_h^2} C^{\mu e*}_{\rm EH} \tag{A11}$$

$$C^{bb}_{S,LL} = -\frac{m_b v}{m_h^2} C^{\mu e*}_{\rm EH} \tag{A12}$$

$$C^{cc}_{S,RR} = C^{e\mu cc}_{\rm LEQU} - \frac{m_c v}{m_h^2} C^{e\mu}_{\rm EH} \tag{A13}$$

$$C^{bb}_{S,RR} = -\frac{m_b v}{m_h^2} C^{e\mu}_{\rm EH} \tag{A14}$$

$$C^{cc}_{S,LR} = -\frac{m_c v}{m_h^2} C^{\mu e*}_{\rm EH} \tag{A15}$$

$$C^{bb}_{S,LR} = C^{*\mu ebb}_{\rm LEDQ} - \frac{m_b v}{m_h^2} C^{\mu e*}_{\rm EH} \tag{A16}$$

$$C^{cc}_{S,RL} = -\frac{m_c v}{m_h^2} C^{e\mu}_{\rm EH} \tag{A17}$$

$$C^{bb}_{S,RL} = C^{e\mu bb}_{\rm LEDQ} - \frac{m_b v}{m_h^2} C^{e\mu}_{\rm EH} \tag{A18}$$

$$\frac{C_{FF,R}}{v} = -\frac{\alpha}{9\pi m_t}\left(C^{e\mu tt}_{\rm LEQU} - \frac{2m_t v}{m_h^2} C^{e\mu}_{\rm EH}\right) \tag{A19}$$

$$\frac{C_{GG,R}}{v} = -\frac{\alpha_s}{24\pi m_t}\left(C^{e\mu tt}_{\rm LEQU} - \frac{2m_t v}{m_h^2} C^{e\mu}_{\rm EH}\right) \tag{A20}$$

where $s_W = \sin\theta_W$, all the masses and couplings are running, and are evaluated at the weak scale. The two-loop Barr-Zee diagrams involving top and W loops were included in the matching to the dipole, and the top loop matching the scalar operators onto FF and GG was included for these operators.

These coefficients then run down to the experimental scale with the RGEs of QED × QCD (see, e.g., [36]). QCD effects are numerically significant, although they only renormalize the coefficients.[5] The scalar quark operators run like quark masses, and the operator $\mathcal{O}_{GG,X}$ runs like the gluon kinetic term, which is accounted for by the wave function renormalization of the gluons. So the running parameters in the coefficient are evaluated at the matching scale.

Retaining only the contribution of the flavor-changing Higgs couplings, we obtain

$$\begin{aligned} C^{e\mu}_{D,R} &\simeq \left[C^{e\mu}_{e\gamma} + \frac{e\alpha_e y_t^2}{8\pi^3 y_\mu} C^{e\mu}_{\rm EH}\right]\left[1 - \frac{4\alpha_e}{\pi}\ln\left(\frac{m_W}{m_\mu}\right)\right] + \cdots \\ C_{GG,R} &= \frac{v^2}{12\pi m_h^2} C^{e\mu}_{\rm EH}[\alpha_s(m_t) + \alpha_s(m_b) + \alpha_s(m_c)] + \cdots \\ C_{FF,R} &= \frac{\alpha_e v^2}{6\pi m_h^2} C^{e\mu}_{\rm EH}\left[\frac{9}{3} + 1\right] + \cdots \end{aligned} \tag{A21}$$

where on the right appear SMEFT coefficients evaluated at m_W, and the coefficients on the left can be input into the rate for $\mu \to e$ conversion. Here $C^{e\mu}_{e\gamma} = c_W C^{e\mu}_{\rm EB} - s_W C^{e\mu}_{\rm EW}$.

Combining with Eq. (26), one sees that the contribution of the LFV Higgs interactions $\mathcal{O}^{e\mu}_{\rm EH}$ via $\mathcal{O}_{GG,X}$ is of opposite sign and $\frac{1}{3}$ the magnitude of the dipole contribution. The contribution via the light quark (u, d, s) scalar operators is slightly smaller than the GG contributions and of same sign, which worsens the sensitivity of $\mu \to e$ conversion to $\mathcal{O}_{\rm EH}$.[6] Including both effects, μAu $\to$ e + Au cannot see

$$C^{e\mu}_{\rm EH} \leq 4.7 \times 10^{-5} \tag{A22}$$

whereas including only the dipole would give a sensitivity of $\lesssim 1.6 \times 10^{-5}$.

APPENDIX B: NUMERICAL VALUES OF OVERLAP INTEGRAL

In Table III, we show the numerical values of F_A, defined in Sec. III. A few nuclei are modeled by both the 2pF and 3pG distributions (14) [25], in which case we give the results with the latest distribution: 3pG for $Z = 16$, 28, 38, 40, 42, 50, 56, and 83, and 2pF for other nuclei.

[5]QCD can also mix $\mathcal{O}_{GG,X}$ to $\mathcal{O}_{S,XL} + \mathcal{O}_{S,XR}$ by attaching the gluons to heavy quark line with a mass insertion. But we do not include this, because the scalar operators always have to be matched back to $\mathcal{O}_{GG,X}$ in order to contribute to $\mu \to e$ conversion.

[6]This cancellation is more effective for light targets like Aluminium or Titanium.

TABLE III. F_A for each nucleus.

Nucleus	$F_A \times 10^4$	Nucleus	$F_A \times 10^4$
${}^{19}_{9}$F	1.5	${}^{90}_{40}$Zr	−0.67
${}^{20}_{10}$Ne	1.7	${}^{93}_{41}$Nb	−1.3
${}^{24}_{12}$Mg	2.7	${}^{98}_{42}$Mo	−4.0
${}^{27}_{13}$Al	3.8	${}^{114}_{48}$Cd	−13
${}^{28}_{14}$Si	4.5	${}^{115}_{49}$In	−11
${}^{31}_{15}$P	4.3	${}^{120}_{50}$Sn	−15
${}^{32}_{16}$S	5.0	${}^{121}_{51}$Te	−14
${}^{40}_{18}$Ar	5.6	${}^{138}_{56}$Ba	−25
${}^{40}_{20}$Ca	7.4	${}^{139}_{57}$La	−25
${}^{48}_{22}$Ti	7.1	${}^{142}_{60}$Nd	−29
${}^{51}_{23}$V	7.1	${}^{152}_{62}$Sm	−32
${}^{52}_{24}$Cr	7.2	${}^{165}_{67}$Ho	−40
${}^{55}_{25}$Mn	8.3	${}^{181}_{73}$Ta	−46
${}^{56}_{26}$Fe	7.5	${}^{184}_{74}$W	−51
${}^{59}_{27}$Co	7.5	${}^{197}_{79}$Au	−61
${}^{58}_{28}$Ni	7.8	${}^{208}_{82}$Pb	−63
${}^{63}_{29}$Cu	6.6	${}^{209}_{83}$Bi	−65
${}^{64}_{30}$Zn	6.2	${}^{232}_{90}$Th	−74
${}^{88}_{38}$Sr	−0.26	${}^{238}_{92}$U	−75
${}^{89}_{39}$Y	−0.37	…	…

[1] Y. Kuno and Y. Okada, Muon decay and physics beyond the standard model, Rev. Mod. Phys. **73**, 151 (2001).

[2] Y. G. Cui *et al.* (COMET Collaboration), Conceptual design report for experimental search for lepton flavor violating $\mu^- \to e^-$ conversion at sensitivity of 10^{-16} with a slow-extracted bunched proton beam (COMET), Report No. KEK-2009-10, 2009; R. Abramishvili *et al.* (COMET Collaboration), COMET phase-I technical design report, Prog. Theor. Exp. Phys. 033C01 (2020).

[3] R. M. Carey *et al.* (Mu2e Collaboration), Proposal to search for $\mu^- N \to e^- N$ with a single event sensitivity below 10^{-16}, Report No. FERMILAB-PROPOSAL-0973, 2008; L. Bartoszek *et al.* (Mu2e Collaboration), Mu2e technical design report, arXiv:1501.05241.

[4] A. Blondel *et al.* (Mu3e Collaboration), Research proposal for an experiment to search for the decay $\mu \to eee$, arXiv:1301.6113.

[5] A. M. Baldini *et al.* (MEG Collaboration), Search for the lepton flavour violating decay $\mu^+ \to \mathrm{e}^+\gamma$ with the full dataset of the MEG experiment, Eur. Phys. J. C **76**, 434 (2016).

[6] P. W. Cattaneo *et al.* (MEG II and MU3E Collaborations), MEG II and Mu3e status and plan, EPJ Web Conf. **212**, 01004 (2019).

[7] R. D. Bolton *et al.*, Search for rare muon decays with the crystal box detector, Phys. Rev. D **38**, 2077 (1988).

[8] U. Bellgardt *et al.* (SINDRUM Collaboration), Search for the decay $\mu^+ \to e^+e^+e^-$, Nucl. Phys. **B299**, 1 (1988).

[9] W. H. Bertl *et al.* (SINDRUM II Collaboration), A Search for muon to electron conversion in muonic gold, Eur. Phys. J. C **47**, 337 (2006); C. Dohmen *et al.* (SINDRUM II Collaboration), Test of lepton flavor conservation in $\mu \to e$ conversion on titanium, Phys. Lett. B **317**, 631 (1993).

[10] Y. Kuno *et al.* (PRISM Collaboration), An experimental search for a $\mu N \to eN$ conversion at sensitivity of the order of 10^{-18} with a highly intense muon source: PRISM (to be published), Report No. J-PARC LOI, 2006.

[11] J. D. Bowman, T. P. Cheng, L. F. Li, and H. S. Matis, New Upper Limit for $\mu \to e\gamma\gamma$, Phys. Rev. Lett. **41**, 442 (1978).

[12] M. Pospelov and T. ter Veldhuis, Direct and indirect limits on the electromagnetic form-factors of WIMPs, Phys. Lett. B **480**, 181 (2000).

[13] N. Weiner and I. Yavin, How dark are majorana WIMPs? Signals from MiDM and rayleigh dark matter, Phys. Rev. D **86**, 075021 (2012).

[14] M. T. Frandsen, U. Haisch, F. Kahlhoefer, P. Mertsch, and K. Schmidt-Hoberg, Loop-induced dark matter direct detection signals from gamma-ray lines, J. Cosmol. Astropart. Phys. 10 (2012) 033.

[15] G. Ovanesyan and L. Vecchi, Direct detection of dark matter polarizability, J. High Energy Phys. 07 (2015) 128.

[16] L. Calibbi, D. Redigolo, R. Ziegler, and J. Zupan, Looking forward to lepton-flavor-violating ALPs, arXiv:2006.04795.

[17] J. Jaeckel and A. Ringwald, The low-energy frontier of particle physics, Annu. Rev. Nucl. Part. Sci. **60**, 405 (2010).

[18] A. M. Baldini *et al.* (MEG Collaboration), Search for lepton flavour violating muon decay mediated by a new light particle in the MEG experiment, Eur. Phys. J. C **80**, 858 (2020).
[19] E. Abouzaid *et al.* (KTeV Collaboration), Search for Lepton Flavor Violating Decays of the Neutral Kaon, Phys. Rev. Lett. **100**, 131803 (2008).
[20] See, eg, chapter 19 of M. E. Peskin and D. V. Schroeder, *An Introduction to Quantum Field Theory* (Addison-Wesley, Reading, USA, 1995), p. 842.
[21] M. A. Shifman, A. I. Vainshtein, and V. I. Zakharov, Remarks on Higgs boson interactions with nucleons, Phys. Lett. **78B**, 443 (1978).
[22] V. Cirigliano, R. Kitano, Y. Okada, and P. Tuzon, On the model discriminating power of $\mu \to e$ conversion in nuclei, Phys. Rev. D **80**, 013002 (2009).
[23] R. Kitano, M. Koike, and Y. Okada, Detailed calculation of lepton flavor violating muon electron conversion rate for various nuclei, Phys. Rev. D **66**, 096002 (2002); Erratum, Phys. Rev. D **76**, 059902 (2007).
[24] M. E. Rose, *Relativistic Electron Theory* (John Wiley & Sons, New York, 1961).
[25] C. W. De Jager, H. De Vries, and C. De Vries, Nuclear charge- and magnetization-density-distribution parameters from elastic electron scattering, At. Data Nucl. Data Tables **14**, 479 (1974).
[26] J. Bellicard, P. Leconte, T. H. Curtis, R. A. Eisenstein, D. Madsen, and C. Bockelman, The scattering of 60 MeV electrons from 90Zr, Nucl. Phys. **A143**, 213 (1970).
[27] A. L. Fitzpatrick, W. Haxton, E. Katz, N. Lubbers, and Y. Xu, The effective field theory of dark matter direct detection, J. Cosmol. Astropart. Phys. 02 (2013) 004.
[28] T. Suzuki, D. F. Measday, and J. P. Roalsvig, Total nuclear capture rates for negative muons, Phys. Rev. C **35**, 2212 (1987).
[29] S. Borsanyi, Z. Fodor, C. Hoelbling, L. Lellouch, K. K. Szabo, C. Torrero, and L. Varnhorst, Ab-initio calculation of the proton and the neutron's scalar couplings for new physics searches, arXiv:2007.03319.
[30] M. Hoferichter, J. Ruiz de Elvira, B. Kubis, and U. G. Meißner, High-Precision Determination of the Pion-Nucleon Term from Roy-Steiner Equations, Phys. Rev. Lett. **115**, 092301 (2015).
[31] J. M. Alarcon, J. Martin Camalich, and J. A. Oller, The chiral representation of the πN scattering amplitude and the pion-nucleon sigma term, Phys. Rev. D **85**, 051503 (2012).
[32] J. M. Alarcon, L. S. Geng, J. Martin Camalich, and J. A. Oller, The strangeness content of the nucleon from effective field theory and phenomenology, Phys. Lett. B **730**, 342 (2014).
[33] P. Junnarkar and A. Walker-Loud, Scalar strange content of the nucleon from lattice QCD, Phys. Rev. D **87**, 114510 (2013).
[34] S. Davidson, Completeness and Complementarity for $\mu \to e\gamma$, $\mu \to 3e$ and $\mu \to e$ conversion, arXiv:2010.00317.
[35] S. Davidson, $\mu \to e\gamma$ and matching at m_W, Eur. Phys. J. C **76**, 370 (2016).
[36] A. Crivellin, S. Davidson, G. M. Pruna, and A. Signer, Renormalisation-group improved analysis of $\mu \to e$ processes in a systematic effective-field-theory approach, J. High Energy Phys. 05 (2017) 117.
[37] M. Ciuchini, E. Franco, L. Reina, and L. Silvestrini, Leading order QCD corrections to $b \to s\gamma$ and $b \to sg$ gluon decays in three regularization schemes, Nucl. Phys. **B421**, 41 (1994).
[38] B. Grzadkowski, M. Iskrzynski, M. Misiak, and J. Rosiek, Dimension-six terms in the Standard Model lagrangian, J. High Energy Phys. 10 (**2010**) 085.